Er$_2$O$_3$ coating by reactive magnetron sputtering: Effect of oxygen supply and erbium pre-layer deposition

P.A. Rayjada [a,*], N.P. Vaghela [a], R. Rahman [a], M. Bhatnagar [a], M. Ranjan [a], N.L. Chauhan [a],
Amit Sircar [a], L.M. Manocha [b], P.M. Raole [a]

[a] Institute for Plasma Research, Bhat, Gandhinagar, 382428, India
[b] DMSRD Establishment, Kanpur, India

ABSTRACT

Erbium oxide (erbia/Er$_2$O$_3$) is one of the leading candidate coating types to address the issues of tritium permeation reduction and Magnetohydrodynamic (MHD) drag reduction in fusion reactor with liquid Lead–Lithium (Pb–Li) or molten salt Flibe ($2LiF + BeF_2$) as the coolant and breeder materials. The electrical resistivity, hydrogen/deuterium permeation reduction property, liquid metal corrosion, radiation effects and deposition techniques are major areas of research on erbia coating. Though it is having a single stable phase of cubic structure up to 2300 °C, it is known to develop metastable monoclinic phase especially in sputter coating methods. We grow erbia by reactive magnetron sputter coating method and study the phase formation, electrical, microstructural and optical dielectric properties. The effects of erbium metal pre-layer deposition, post annealing in oxygen rich vacuum and oxygen to argon gas feed ratio are studied keeping other parameters constant.

The film grows in mixed phase of cubic and monoclinic structures when erbium metal pre-layer is deposited on the P91 steel substrate and in pure monoclinic phase in absence of the pre-layer. Post annealing seems to partially convert monoclinic into cubic phase in the mixed phase coating. Better crystallization and slightly more surface roughness is observed in the sample processed with higher oxygen to argon ratio. DC resistivity is found in 10^{15} Ω∗cm range and it is marginally more in the sample processed with more oxygen. The spectroscopic ellipsometry on these films to obtain optical dielectric properties gives encouraging results in terms of close match of the thickness and roughness values with those obtained from SEM and AFM respectively. Systematic study of optical dielectric property suggests a trend consistent with DC resistivity.

1. Introduction

Tritium containment is extremely important in fusion fuel cycle due to the human and structural material safety issues and accountability of bred tritium, which is invaluable fuel and needs to be extracted in the most effective way. This is challenging in a blanket systems with Pb–Li eutectic and molten salt Flibe ($2LiF + BeF2$) breeder based designs, which is supposed to have high concentration of tritium [1]. Another issue is that of Magnetohydrodynamic (MHD) drag induced pressure drop in liquid metal flow across heavy magnetic fields [2,3]. To address these two issues

of MHD drag and tritium confinement, a suitable ceramic coating on the inner surface of the volume is suggested [4].

AlN, Al$_2$O$_3$, Er$_2$O$_3$, Y$_2$O$_3$, etc., are being actively explored by the fusion materials research community world over for this purpose [5]. For Er$_2$O$_3$ coatings, substrate oxidation is one of the important factor ascribed for coating instability [6,7]. Er$_2$O$_3$ coating is deposited by various methods such as filtered vacuum arc [8], RF magnetron sputtering [9], reactive magnetron sputtering [10] metal organic decomposition [11,12] etc. Its electrical resistivity, permeation reduction factor (PRF) for hydrogen and deuterium and compatibility with liquid lithium and Pb–Li are the issues at the focus of the researchers. The resistivity is reported in the range of 10^7– 10^{14} Ω∗cm for measuring temperature of 800 °C to room temperature, respectively [6,13]. The PRF with erbia coating is also reported to be more than 1000, which is better than the required value [14].

* Corresponding author. Institute for Plasma Research, Near Indira Bridge, Bhat, Gandhinagar, 382428, India.
E-mail address: pratipalsinh@gmail.com (P.A. Rayjada).

Table 1
Samples details with variation in process parameters.

O$_2$/Ar feed ratio	Sample-1	Sample-2	Sample-3	Sample-4
0.25	Er pre-layer, 2 h deposition @ 500 °C	Er pre-layer, 2 h deposition + 1 h annealing @ 500 °C		No Er pre-layer, 2 h deposition + 1 h annealing @ 600 °C
0.40			Er pre-layer, 2 h deposition + 1 h annealing @ 500 °C	

In this study, we deposit Er$_2$O$_3$ coating on P91 grade steel, which is very close to Reduced Activation Ferritic Martensitic Steel (RAFMS), the structural material for the blanket, in terms of structure, microstructure and composition. The crystal structure phases, electrical resistivity, surface topology, cross-sectional imaging and optical dielectric properties are studied using X-ray Diffraction (XRD), Electrometer, Atomic Force Microscopy (AFM), Scanning Electron Microscopy (SEM) and Spectroscopic Ellipsometry and compared among the films deposited at varying processing conditions. Especially, the effects of oxygen supply and metallic pre-layer are studied.

2. Experimental

Reactive magnetron sputter coating of erbia on P91 grade stainless steel substrates were carried out using a 3″ planar magnetron system developed in house. The P91 steel substrates of 25 × 25 × 5 mm size were mirror polished and ultrasonically cleaned in acetone before loading into the deposition chamber. In order to ensure a clean interface, the substrates were in-situ sputter cleaned prior to deposition. Substrates were kept at alleviated process temperatures (500/600 °C) during the sputter cleaning, deposition and post annealing in oxygen rich vacuum. The deposition was carried out for 2 hours. First 90 seconds, erbium pre-layer was coated by allowing the sputtering of erbium target with pure argon plasma. Subsequently, oxygen was introduced and reactive oxide coating was allowed for the rest of the time. The process was stable, consistent and reproducible with 1.0×10^{-2} mbar pressure, cathode power of 200 W and target substrate distance of about 12 cm. The process was systematically repeated to make 4 samples as listed in Table 1.

The coatings were analysed using powder mode XRD (Seifert make XRD3000PTS) with Cu Kα source, DC Electrical resistivity (Keithley make Electrometer 6517B), contact mode AFM (NT-MDT, NTEGRA), SEM at 50,000× magnification (LEO440i) and Spectroscopic Ellipsometry in 400–1100 nm range (J. A. Woollam Co).

3. Results and discussion

Having established consistency and reproducibility of the deposition experiments, we obtain highly smooth and stable coatings on P91 steel substrate, which is a close chemical analogue to Indian RAFMS, proposed to be the blanket structural material. The coatings were purple or pinkish in colour indicating the characteristic of erbia. Based on our earlier experience [10], we narrowed down to deposit on only two variants of O$_2$/Ar ratios, namely 0.25 and 0.4 with objective of studying growth of stable cubic phase coating at around 500 °C temperature. Another variation in the process that we report here is introduction of metallic erbium pre-layer, which may improve the stability by bridging the thermal and elastic mismatch between oxide and metallic substrate [15,16] in addition to preventing the substrate oxidation, which is a critical issue for the stability of coating [6,7]. We study the films deposited at 500 °C and 0.25 O$_2$/Ar ratio for the effects of post annealing in oxygen rich vacuum and then compare them with that deposited at 0.40 ratio. The powder mode XRD patterns of samples
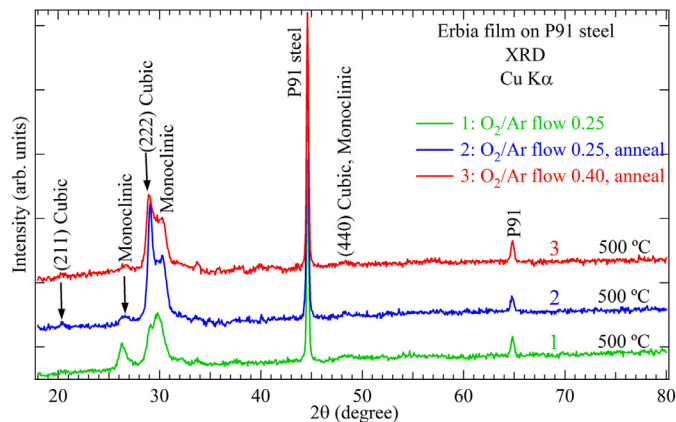

Fig. 1. XRD patterns of sample-1, 2 and 3 with constant relative vertical offset.

1–3 are shown in Fig. 1 with vertical offset for clarity. The patterns clearly show that the films are consisting of cubic as well as monoclinic phases. The phase identification is performed by comparing the observed patterns with JCPDS standard pattern of cubic phase [17] and simulated pattern of monoclinic phase [10]. Cubic phase of erbium oxide is thermally stable up to 2300 °C whereas monoclinic is a metastable phase that can form under high pressure. Sputter coated films are inherently residually stressed and this may stimulate formation of monoclinic phase as reported earlier [10]. Though there are strong overlaps among the peaks of cubic and monoclinic phases, fortunately there is one unique peak from each phase. The peak at ~20.60° is a clean (2 1 1) peak of cubic phase and one at 26.75° is of monoclinic phase. Moreover, (2 2 2) cubic peak at 29.27° and partially overlapping bunch of monoclinic peaks extending up to 30.53° also show significant evidence to help us distinguish the two phases. Close observation reveals that sample-1 consists of dominantly monoclinic phase, whereas contribution from cubic phase dominates in sample-2. This suggests that post annealing for 1 h is significantly transforming the metastable phase into cubic phase, but not completely. However, post annealing on sample-3 processed with higher oxygen availability is relatively less effective in increasing the cubic phase content any more. The clean monoclinic peak of sample-1 (26.26°) is shifted to lower angle as compared to positions of simulated room temperature monoclinic phase (26.75°) and the shift gets systematically reduced for sample-2 (26.54°) and sample-3 (26.68°) indicating that post annealing and higher oxygen availability reduces the compressive residual stress in this phase. On the other hand, cubic (2 2 2) peak at ~29° is nearly unchanged and is slightly at lower angle as compared to the normal position (29.27°), indicating that the cubic phase is also under compressive stress and it is not changing significantly with this variations of process.

Furthermore, we analyse the surface topology and microstructure using atomic force microscopy on sample-2 and sample-3 to study the effect of higher oxygen availability at 500°C processing temperature. Fig. 2 shows the AFM images of the two samples on 3 × 3 μm area. Relative study indicates that more oxygen in sample-3 processing leads to larger crystallites of upto about
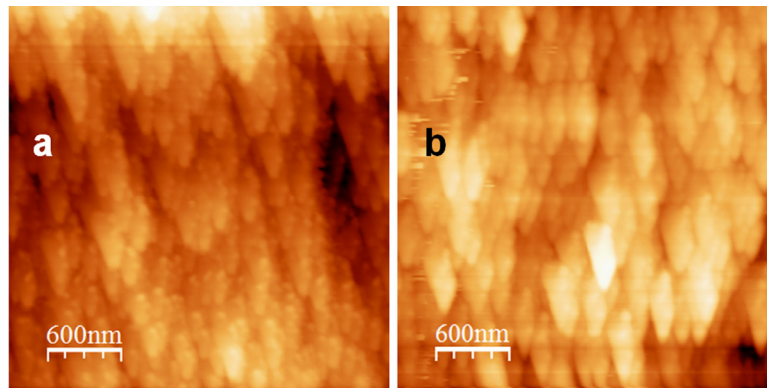
Fig. 2. AFM image on 3×3 micron area of (a) sample-2 and (b) sample-3.
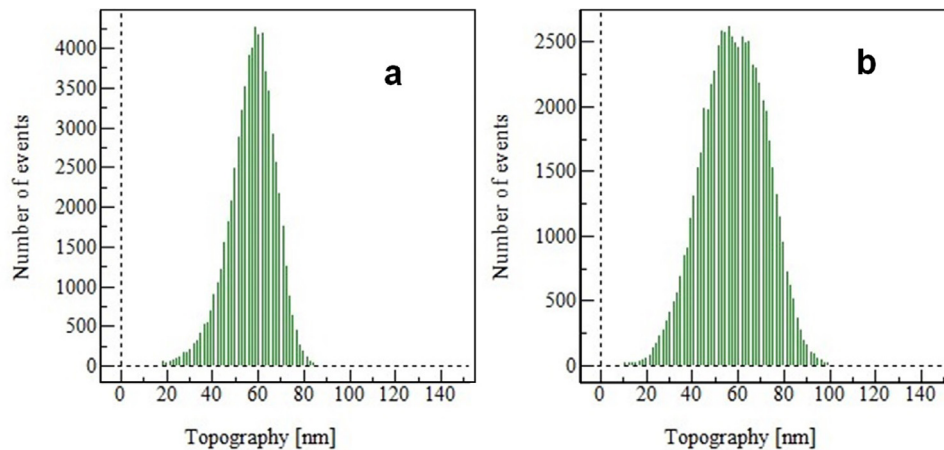

Fig. 3. Roughness analysis derived from AFM analysis of (a) sample-2 and (b) sample-3.

500 nm size growing vertically. The crystallites in sample-2 are relatively smaller and many fine particles of about 50 nm size are attached to the main crystallites. This indicates better crystallization in sample-3. This combined with the XRD observations, suggest that higher oxygen availability gives better crystallization but largely of monoclinic phase.

These observations are substantiated by roughness analysis of these samples shown in Fig. 3. It clearly shows that maximum (peak-to-peak) roughness of sample-3 is more than 100 nm, which is significantly higher than ~80 nm roughness in sample-2. The RMS roughness of sample-2 and sample-3 are 10.3 and 14.5 nm respectively, confirming that more oxygen availability in reactive deposition contributes to surface roughness, probably due to better crystallization.

The DC electrical resistivity of the coatings was measured using Keithley's 6517B electrometer and a special fixture. The bottom of the substrate was polished for firm electrical contact with the bottom electrode plate and conducting tape of 3×3 mm was applied on the film for contact with the top electrode. The sample was charged with 60 V to measure small value of current with the electrometer. Resistivity was evaluated using the size of the electrode and thickness of the film. Fig. 4 shows the bar chart of the resistivity of sample-2 and sample-3. It is of the order of 10^{15} Ω^*cm and is somewhat on the higher side of the reported values of the order of 10^{14} Ω^*cm[12]. The higher value for sample-3 as compared to sample-2 may be due to better crystallization as indicated by the AFM topology.

Surface and cross-section SEM images of the coating on silicon wafers deposited along with the deposition of sample-2 (0.25 O_2/Ar ratio) and sample-3 (0.4 O_2/Ar ratio) at 50,000 magnifica-
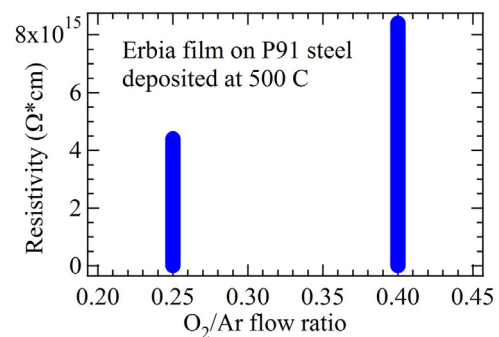

Fig. 4. Bar chart of DC resistivity of Erbia film processed at 500°C with different O_2/Ar flow.

tion are shown in Fig. 5. The morphology of the surface and cross-sections obtained looks more or less similar for both of them. The typical columnar structure seen in the cross-section of sputter deposited crystalline films is not evident in these films indicating over all weak crystallization. The cross-section SEM imaging was used for precisely determining the thickness of the coatings. Somewhat smaller thickness of sample-3 is due to higher oxygen availability as the deposition rate is known to reduce in reactive sputtering mode as compared to metallic sputtering mode. The thickness values were used as inputs for resistivity evaluation and fitting program of Ellipsometry data as described later in this section.

In order to gain more understanding on phase formation mechanism of the erbia coating, a special experiment was done
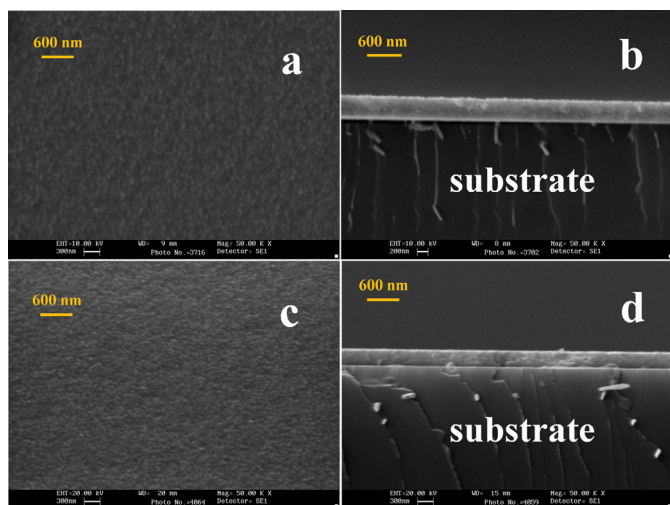
Fig. 5. Scanning Electron Micrographs: sample-2 (a) surface and (b) cross-section, sample-3 (c) surface and (d) cross-section.
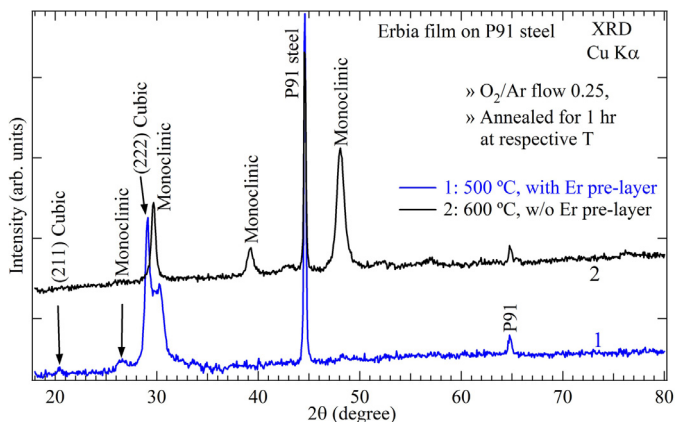

Fig. 6. XRD patterns of sample-2 and 4 with constant relative vertical offset.

without erbium metallic pre-layer deposition and substrate temperature raised to 600 °C with post annealing for 1 h at 600 °C. The O_2/Ar feed ratio was 0.25. The coating prepared is named sample-4 in this study. Fig. 6 compares powder XRD pattern of this coating with that of sample-2 processed with Er pre-layer at 500 °C, having the remaining parameters unchanged. The pattern of sample-4 clearly shows all the peaks characteristic of monoclinic phase with good intensity. Even additional monoclinic phase peaks at ∼39° and ∼48° are prominent, which are absent in the previous three samples processed at 500 °C. This clearly suggests higher degree of crystallization due to higher processing and post annealing temperature. However, the most striking feature is complete absence of cubic phase (no (2 1 1) or (2 2 2) peaks) in sample-4 in-spite of higher processing and post annealing temperature. This result clearly shows that cubic phase formation is nucleated or initiated from the erbium metallic pre-layer upon heat treatment under oxygen availability as evidenced by the (2 1 1) peak at ∼20.38° and (2 2 2) peak at ∼29° in sample-2 and sample-3 (Figs. 1 and 6). Cubic phase can not be formed by reactive sputter coating at least upto 600 °C substrate temperature. Earlier, we have reported [10] cubic phase formation even at 360 °C substrate temperature, but in a narrow window of O_2/Ar flow ratio around very small value of 0.056 to 0.088. In the light of these new results, we understand that the cubic phase formed there would also be due to metallic erbium sputtering due to lack of sufficient oxygen content in processing. In a recent study on Y_2O_3 coating by reactive

sputter deposition, a similar behaviour is observed, where cubic phase is readily obtained with low oxygen processing characterized as metallic sputtering mode [18]. However, with high oxygen processing, characterized as reactive sputtering mode, the coating showed cubic phase only after it was subjected to post annealing for 15 h at 600 °C. Cubic phase is stable upto 2300 °C whereas monoclinic is a metastable phase which converts into cubic when exposed to sufficiently high temperature. The atomic number normalized unit cell volume of the cubic phase is about 9% larger than that of a monoclinic phase [19] and this can lead to the cracking of the coating upon such phase transition. The deuterium PRF has been shown to be inferior for monoclinic erbia coating on Eurofer as compared to cubic erbia coating [20].

For further characterization of the dielectric properties of the coating, we applied reflection based spectroscopic ellipsometry in incident wavelength range of 400 nm to 1100 nm with a step size of 2 nm. It is non-destructive optical technique, which can give information about the optical dielectric constants and refractive index of the coating. Since AC conductivity is linked with the imaginary part of the ac dielectric constant ($\sim\lambda*\sigma$/c), it would be interesting to explore such a technique. If sufficiently studied, the dielectric response and DC conductivity can be correlated for a given material coating and subsequently DC conductivity can easily be evaluated by optical means without damaging the film by electrode coating, etc. Moreover, this technique can also estimate refractive index, thickness, surface roughness of the film. It would be interesting to correlate refractive index with the phase content of the film.

Spectroscopic Ellipsometry measures the amplitude ratio (Ψ) and phase difference (Δ) of the reflection coefficients of p- and s- polarized light which are related to complex refractive index of sample through Fresnel's equations [21]. The p- and s- components polarized light are irradiated onto a sample at Brewster angle, where the difference between the two reflection coefficients of p- and s- polarized light is maximum. Due to the difference in electric dipole radiation from p- to s- direction, the amplitude of reflection coefficients is significantly different. For a homogeneous sample, refractive index and extinction coefficients can be calculated with measured (Ψ, Δ) values by using Fresnel's equations [21]. The reflection coefficients are related to Ψ and Δ by a parameter ρ as shown below [21].

$$\rho \equiv \tan(\psi)\exp(i\Delta) \equiv \frac{r_p}{r_s} \equiv \left(\frac{E_{rp}/E_{ip}}{E_{rs}/E_{is}}\right)$$

Here E_{rp} and E_{ip} denote reflected and incident electric field vectors for p- polarized light, respectively. Similarly E_{rs} and E_{is} are reflected and incident electric field vectors for s- polarized light wave, respectively. The p- polarized component of the incident wave lies in the plane of incidence whereas the s- polarized component lies perpendicular to the plane of incidence.

To analyse the measured ellipsometric data, a physical model is defined for the dielectric function ε. Then Ψ and Δ are calculated with the help of the physical model by introducing known dielectric functions as the starting point. The calculated and the measured values of Ψ and Δ are compared. A mean-square error minimization algorithm [22] is used to get the best fit between model and measured values which leads to physically acceptable dielectric constants and the thickness of the thin film. The thickness obtained for sample-2 and sample-3 are 408.75 nm and 375 nm, respectively, which reasonably matched with the corresponding actual thickness of 423.4 and 315 nm measured through SEM. Fig. 7 shows the measured and modelled Ψ and Δ after fitting of a four layer model to the experimental data of sample-2 as a representative (see Fig. 7(b). Fit statistics were checked to ensure that there was no correlation between the parameters used in the model. The intermix layer of 29.56 nm is likely due to the roughness of the
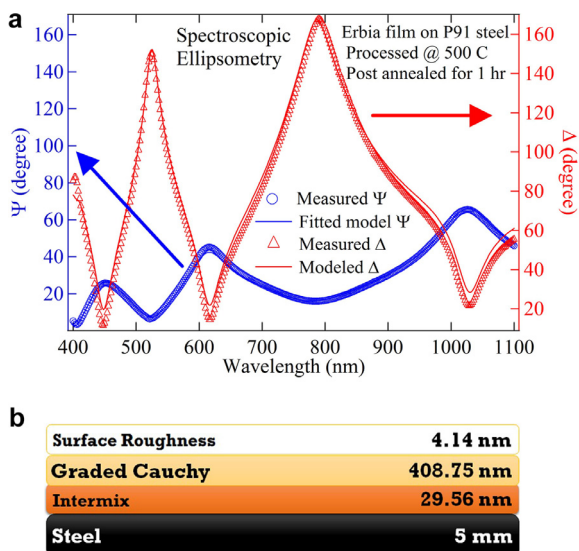
Fig. 7. (a) Ψ and Δ of the erbia thin film deposited on a P91 in sample-2, (b) Scheme of model fitted to the ellipsometry data of sample-2. The four layer model for erbia coating on P91 steel.
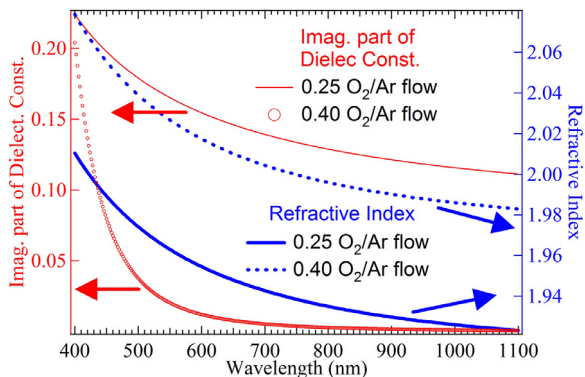

Fig. 8. Imaginary part of dielectric constant (red) and optical refractive index (blue) as a function of wavelength for sample-2 and 3.

substrate. The top roughness obtained by the model for sample 2 and 3 are 4.14 nm and 12.6 nm, respectively and they correlate pretty well with the RMS roughness values of 10.3 nm and 14.5 nm obtained from AFM study. In general, a Cauchy layer is used to describe the refractive index in the spectral region where the film is transparent, but with addition of Urbach parameters, it is possible to incorporate absorption in the model [23]. Interestingly, the best fit leads to a graded Cauchy layer. This may be due to the metallic erbium pre-layer. The excellent correlation with actual thickness, roughness and fitting quality help us obtain realistic dielectric and optical properties of the film. Fig. 8 shows the imaginary dielectric constant and refractive index of sample-1 and sample-2.

The Imaginary part of dielectric constant (ε_2) and optical refractive index obtained from the model fit for sample-2 and 3 are shown in Fig. 8. Higher values of ε_2 and refractive index at 400 nm wavelength smoothly decay with increasing wavelength. This is typical behaviour of an insulating material. The ε_2 of sample-3 is almost two orders of magnitude lower than that of sample-2 (at ~1000 nm). As discussed above, ε_2 roughly scales with the conductivity ($\sim\lambda*\sigma/c$). Though the difference in ε_2 is too much as compared to the difference observed in DC resistivity, it does support qualitatively the resistivity results that sample-3 should have

higher resistivity than sample-2. The higher values of refractive index for sample-3 also suggest that processing with higher oxygen leads to more effective chemical reaction for the Er_2O_3 formation.

4. Conclusions

The effects of post annealing in oxygen rich vacuum, erbium metal pre-layer deposition and oxygen to argon gas feed ratio on erbia film processing are systematically studied at 500 °C processing temperature. Coating is found to grow in mixed phase of cubic and monoclinic structures when erbium metal pre-layer is deposited and in pure monoclinic phase in absence of the pre-layer. It remains in pure monoclinic phase even at 600 °C if erbium pre-layer is not deposited. Annealing helps to partially convert monoclinic into cubic phase but only if cubic phase is present. Higher oxygen supply in reactive deposition leads to more of monoclinic phase formation and better crystallization with slightly higher surface roughness. DC resistivity is also slightly more for such sample as compared to one which is prepared at the same parameters but lesser oxygen availability. We try to study the spectroscopic ellipsometry on the films to obtain optical dielectric properties for correlation with DC conductivity. The results are encouraging as it gives matching thickness and roughness values with those obtained from SEM and AFM respectively. The dielectric results are also showing trend consistent to resistivity but more experiments would be required to get quantitative agreement. It would be interesting to extend this study to further understand the phase formation dynamics and its correlation with the dielectric properties and DC resistivity at higher temperatures.

References

[1] T. Shikama, R. Knitter, J. Konys, T. Muroga, K. Tsuchiya, A. Moesslang, H. Kawamura, S. Nagata, Fusion Eng. Des. 83 (2008) 976.
[2] T. Muroga, J.M. Chen, V.M. Chernov, K. Fukumoto, D.T. Hoelzer, R.J. Kurtz, T. Nagasaka, B.A. Pint, M. Satou, A. Suzuki, H. Watanabe, J. Nucl. Mater. 367–370 (2007) 780.
[3] Hidetoshi Hashizume, Fusion Eng. Des. 81 (2006) 1431.
[4] B.A. Pint, P.F. Tortorelli, A. Jankowski, J. Hayes, T. Muroga, A. Suzuki, O.I. Yeliseyeva, V.M. Chernov, J. Nucl. Mater. 329–333 (2004) 119–124.
[5] A. Sawada, T. Terai, A. Suzuki, M. Yamawaki, J. Phys. Chem. Solids 66 (2005) 681–683.
[6] T. Tanaka, T. Muroga, Fusion Eng. Des. 88 (2013) 2569.
[7] D. Zhang, T. Tanaka, T. Muroga, Fusion Sci. Technol. 60 (2011) 1576.
[8] Y. Yamada-Takamura, F. Koch, H. Maier, H. Bolt, Surf. Coat. Technol. 142–144 (2001) 260–264.
[9] Akihiko Sawada, Akihiro Suzuki, Takayuki Terai, Fusion Eng. Des. 81 (2006) 579.
[10] P.A. Rayjada, N.P. Vaghela, N.L. Chauhan, A. Sircar, E. Rajendrakumar, L.M. Manocha, P.M. Raole, Fusion Sci. Technol. 65 (2014) 194.
[11] Takumi Chikada, Akihiro Suzuki, Teruya Tanaka, Takayuki Terai, Takeo Muroga, Fusion Eng. Des. 85 (2010) 1537.
[12] Dongxun Zhang, Teruya Tanaka, Takeo Muroga, J. Nucl. Mater. 417 (2011) 1249.
[13] D.L. Smith, J. Konys, T. Muroga, V. Evitkhin, J. Nucl. Mater. 307–311 (2002) 1314.
[14] Takumi Chikada, Akihiro Suzuki, Freimut Koch, Hans Maier, Takayuki Terai, Takeo Muroga, J. Nucl. Mater. 442 (2013) S592.
[15] M.T. Vieira, A.S. Ramos, J. Mat. Process. Technol. 92-93 (1999) 156–161.
[16] D.T. Chavara, A.J. Ruys, in: D. Zhu, U. Schulz (Eds.), Advanced Ceramic Coatings and Interfaces, John Wiley & Sons, 2007, p. 311.
[17] JCPDS–International Centre for Diffraction Data, 1995 database, PDF No. 8-50
[18] J. Engels, A. Houben, P. Dollase, M. Köppen, M. Rasinski, Y. Mao, F. Koch, Ch. Linsmeier, Poster presented in 17th International Conference on Fusion Reactor Materials, 11–16 Oct, 2015.
[19] Q.X. Guo, Y.S. Zhao, C. Jiang, W.L. Mao, Z.W. Wang, J.Z. Zhang, Y.J. Wang, Inorg. Chem. 46 (2007) 6164.
[20] A. Brendel, C. Adelhelm, M. Werkstetter, T. Pickert, K. Ertl, M. Balden, M. Rasinski, T. Plocinski, Ch. Linsmeier, 13th International Workshop on Plasma-Facing Materials and Components for Fusion Applications and 1st International Conference on Fusion Energy Materials Science May 9–13, 2011.
[21] H. Fujiwara, Spectroscopic Ellipsometry: Principles and Applications, Wiley, 2007.
[22] J. Nocedal, S.J. Wright, Numerical Optimization, Springer, 1999.
[23] S. John, C. Soukoulis, M.H. Cohen, E.N. Economou, Theory of electron band tails and the Urbach optical-absorption edge, Phys. Rev. Lett. 57 (14) (1986) 1777.